Why the Lysogenic State of Phage λ Is So Stable: A Mathematical Modeling Approach

Moisés Santillán* and Michael C. Mackey†

*Centre for Nonlinear Dynamics, McGill University, H3G 1Y6 Montreal, Quebec, Canada; and †Departments of Physiology, Physics & Mathematics and Centre for Nonlinear Dynamics, McGill University, H3G 1Y6 Montreal, Quebec, Canada

ABSTRACT We develop a mathematical model of the phage λ lysis/lysogeny switch, taking into account recent experimental evidence demonstrating enhanced cooperativity between the left and right operator regions. Model parameters are estimated from available experimental data. The model is shown to have a single stable steady state for these estimated parameter values, and this steady state corresponds to the lysogenic state. When the CI degradation rate (γ_{cI}) is slightly increased from its normal value ($\gamma_{cI} \simeq 0.0$ min^{-1}), two additional steady states appear (through a saddle-node bifurcation) in addition to the lysogenic state. One of these new steady states is stable and corresponds to the lytic state. The other steady state is an (unstable) saddle node. The coexistence these two globally stable steady states (the lytic and lysogenic states) is maintained with further increases of γ_{cI} until $\gamma_{cI} \simeq 0.35$ min^{-1}, when the lysogenic steady state and the saddle node collide and vanish (through a reverse saddle node bifurcation) leaving only the lytic state surviving. These results allow us to understand the high degree of stability of the lysogenic state because, normally, it is the only steady state. Further implications of these results for the stability of the phage λ switch are discussed, as well as possible experimental tests of the model.

INTRODUCTION

Bacteriophage (or simply phage) λ is a virus capable of infecting *Escherichia coli* bacteria. After infection, the virus can follow either one of two different pathways: 1), the virus integrates its DNA into the host bacterial DNA and duplicates when the bacterium divides (this pathway is known as lysogeny); 2), the virus uses the bacterial molecular machinery to make many viral copies and leave (after killing the host bacterium) to infect other bacteria (the so-called lysis pathway). Once the virus is in the lysogenic state, it can shift to the lysis state under certain conditions, e.g., if the bacterial culture is irradiated with ultraviolet (UV) light. The molecular regulatory mechanism responsible for the lysogeny/lysis decision is known as the phage λ switch.

The two patterns of phage λ behavior, lytic and lysogenic, and the subtle ways in which it subverts its host, *E. coli*, have made it a paradigm for many biological pathways (Gottesman, 1999). One of the most striking characteristics of the phage λ switch is the fact that the intrinsic loss rate of λ lysogeny is of the order of 10^{-7} per cell and generation (Aurell et al., 2002; Little et al., 1999; Rozanov et al., 1998). In contrast, the mutation rate in the portion of the λ genome involved in lysogeny is between 10^{-6} and 10^{-7} per generation (Aurell et al., 2002; Little et al., 1999). Thus, the lysogenic state is more stable than the genome itself.

The large volume of experimental data on the behavior of this system and the logical structure underlying the switch performance make it appealing for mathematical modeling. Several mathematical models have been proposed in the last two decades to explain the astonishingly high degree of stability of the phage λ lysogenic state. Nevertheless, to our knowledge, both the stability of the lysogenic state and the efficiency of the switch still lack a proper explanation. The aim of this paper is to offer an explanation of the lysogenic state stability based on a new modeling effort. Below, we briefly review some of the existing models of the phage λ switch before turning to an exposition of our results.

The first model incorporating quantitative biochemical information was proposed by Ackers et al. (1982). This is an equilibrium model that explains the existence of the lytic and lysogenic steady states, but not their relative stability. Later, Shea and Ackers (1985) improved their model making it fully dynamical. This model gave the expected qualitative behavior for stable maintenance of lysogeny, as well as for the induction of lysis. Reinitz and Vaisnys (1990) extended the dynamical model, and found a quantitative inconsistency between their experiments and the model predictions. The most extensive model was developed by McAdams and Shapiro (1995) who included all of the proteins involved in the lysis/lysogeny switch, as well as the genes that become active after the fate of the phage is determined. Arkin et al. (1998) published a model of the λ switch based on a stochastic representation of transcription, translation, and interaction between proteins. They accurately predicted the fraction of lysogens developed after infection. Further, their simulations clearly show how two identical cells in identical conditions, infected with the same number of phage, can still meet different fates. More recently, Aurell and Sneppen (2002) and Aurell et al. (2002) studied the stability of the lysogenic state using a stochastic mathematical model. From their results, they suggested that the current view of the phage λ switch is incomplete, given the difference they

Submitted May 12, 2003, and accepted for publication September 16, 2003.

Address reprint requests to Moisés Santillán, Depto. de Física, Esc. Sup. de Física y Matemáticas, Inst. Politécnico Nal. 07738 México D.F., México. Tel.: +52-55-57296000 ext. 55319; Fax: +52-55-57296000 ext. 55051; E-mail: moyo@esfm.ipn.mx.

Moisés Santillán is currently an invited researcher at Departamento de Matemáticas, Centro de Investigación y Estudios Avanzados del IPN.

0006-3495/04/01/75/10 $2.00

observed between the model predictions and the experimentally observed behavior of a mutant virus strain.

Here, we extend the Shea and Ackers (1985) model to account for recently discovered (Dodd et al., 2001; Ptashne and Gann, 2000) interactions (cooperativity) between regulatory molecules bound at two different operator regions. We pay special attention to the estimation of all of the model parameters from published experimental results. An analysis of the model steady states reveals that under normal conditions it only has one stable steady state, corresponding to lysogeny. When the degradation rate of the protein CI is slightly increased from its normal value (0.0 min^{-1}), two additional steady states appear through a saddle node bifurcation. One of these new steady states is also stable and corresponds to lysis, whereas the other is an (unstable) saddle node. This bistable behavior is maintained with further increases of the CI degradation rate until it reaches $\sim$0.35 min^{-1}, when the saddle node and the lysogenic steady state collide and annihilate each other through a reverse saddle node bifurcation. For even larger degradation CI rates there is only one stable steady state, corresponding to lysis. The consequences of these results on the performance and stability of the phage λ switch are finally discussed.

THE PHAGE λ SWITCH

An excellent review of the molecular regulatory mechanisms in the phage λ switch is given by Ptashne (1986). A schematic representation of the λ switch performance in the lysogenic and lytic steady states is shown in Fig. 1. All of the switch regulatory processes take place in the right operator (O_R), which is composed of three regions designated O_R1, O_R2, and O_R3. The promoter P_R completely overlaps O_R1 and partially overlaps O_R2. RNA polymerase enzymes that bind to the promoter P_R initiate transcription of gene *cro*. Similarly, the promoter P_{RM} completely overlaps O_R3 and partially overlaps O_R2. RNA polymerase enzymes bound to the promoter P_{RM} initiate transcription of the *cI* gene. Dimers of *cI* product (denoted CI_2) can bind to O_R1, O_R2, and O_R3, in order of increasing affinity. Conversely, dimers of *cro* product (denoted Cro_2) bind to O_R3 with the highest affinity, then to O_R2, and finally to O_R1. When CI_2's bind to adjacent O_R locations, they do so cooperatively. Thus, the binding energy when there are CI_2's bound to O_R1 and O_R2 or to O_R2 and O_R3 is smaller (larger in absolute value given that interaction and binding energies are negative) than the sum of the individual binding energies. Recently, Darling et al. (2000b) observed that there is also cooperativity between Cro_2's bound to O_R1 and O_R2, to O_R2 and O_R3, and to O_R1, O_R2, and O_R3. All of the individual-site binding and interaction energies are given in Darling et al. (2000b).

In the lysogenic state (see Fig. 1), gene *cI* is on while gene *cro* is off. Monomers of *cI* product (denoted by CI) spontaneously combine to form dimers CI_2. Similarly,

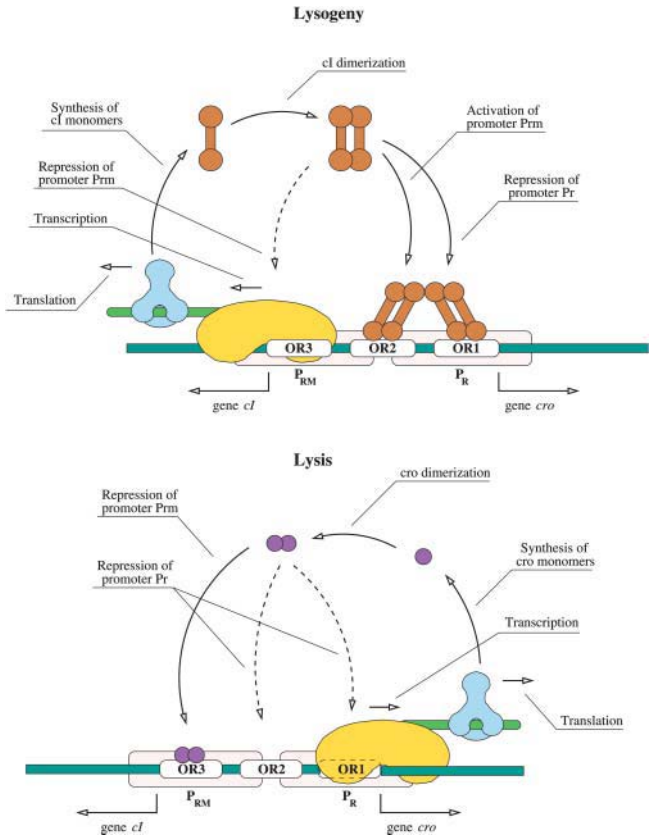

FIGURE 1 A schematic representation of the phage λ switch in the two stable states: lysogeny (*top*) and lysis (*bottom*).

monomers of *cro* product (denoted by Cro) spontaneously form dimers Cro_2. Due to cooperativity, most of the O_R1 and O_R2 sites are occupied by CI_2's in the normal lysogenic state. This has two effects: 1), promoter P_R is repressed (because it is blocked by a CI_2); and 2), the initiation of transcription at promoter P_{RM} is enhanced. One CI_2 bound to O_R2 does not affect the probability that a RNA polymerase will bind promoter P_{RM} and form a closed complex, but it increases the probability for the closed complex to isomerize into an open complex to start transcription. In other words, dimers CI_2 repress the production of Cro and enhance the production of CI. Nevertheless, if the concentration of CI_2 reaches very high values, the probability for CI_2 to bind O_R3 will be increased, which has the effect of repressing RNA polymerase binding to P_{RM}. Thus CI_2 regulates its own concentration by enhancing CI production if its concentration is not too high, and otherwise repressing transcription of gene *cI*.

If the CI_2 concentration decreases, for instance by the cleavage of CI by RecA proteins (activated by UV light), the probability for O_R1 and O_R2 to be free from CI_2 is increased. This, on its own, creates the possibility that a polymerase will bind P_R and start transcription of gene *cro* and, in the long run, leads to an increasing Cro_2 concentration. At a high enough Cro_2 concentration, a Cro_2 can bind O_R3 and repress

CI production, establishing the lytic state. In this state, gene *cro* is on while gene *cI* is off. When the concentration of Cro_2 is too high, a Cro_2 can bind to O_R2 and even to O_R1, repressing the production of Cro.

New experimental evidence (Dodd et al., 2001; Ptashne and Gann, 2000) suggests that there is cooperativity between CI_2's bound to the O_R and O_L operators. As depicted in Fig. 2, the phage λ DNA folds in such a way that CI_2's bound to O_R and O_L sites can interact due to their proximity. Ptashne and Gann (2000) speculate that this newly discovered cooperativity may help explain the incredibly high stability of the lysogenic state.

MODEL DEVELOPMENT

The complex formed by the operator O_R and the promoters P_R and P_{RM} has 40 different binding states. Twenty-seven of these states arise when we consider that O_R1, O_R2, and O_R3 can be either empty, bound by a CI_2, or bound by a Cro_2, giving $3^3 = 27$ different possible combinations without considering the binding of RNA polymerase molecules to promoters P_R and P_{RM}. The fact that whenever O_R3 is free (no matter what the $3^2 = 9$ states of O_R1 and O_R2 are), promoter P_{RM} can be bound by a RNA polymerase, accounts for nine more binding states. Similarly, three more states appear because whenever O_R1 and O_R2 are free (regardless of the state of O_R3 (three combinations)), promoter P_R can be bound by a RNA polymerase. Finally, the last binding state (to complete all 40 of them) is that in which all three O_R1, O_R2, and O_R3 are free and both P_R and P_{RM} are occupied by RNA polymerase molecules.

The left operator of phage λ (O_L) consists of three regions O_L1, O_L2, and O_L3, that can be bound by CI_2 and Cro_2 molecules. There is only one promoter regulated by this operator, promoter P_L. This promoter completely overlaps O_L1 and partially overlaps O_L2. Thus, the left operator-P_L complex has 30 different binding states. Twenty-seven of them arise from the fact that each one of O_L1, O_L2, and O_L3 has three binding states. They can be either free, bound by a CI_2, or bound by a Cro_2. The other three states arise because whenever O_L2 and O_L3 are free, a RNA polymerase molecule can bind P_L, independent of the state of O_L1.

The energy (E_i) of every one of the $40 \times 30 = 1200$ binding states of the complex formed by the right and left operators plus the promoters P_R, P_{RM}, and P_L can be calculated given the cooperativity and individual binding energies of CI_2, Cro_2, and mRNAP. The equation to calculate these energies is:

$$E_i = \sum_{X=R,L}\sum_{Y=CI_2,Cro_2}\sum_{\nu=1}^{3}\Delta G^{Y}_{O_{X^\nu}}\Gamma^{Y}_{O_{X^\nu}}(i) + \sum_{X=R,L}\sum_{Y=CI_2,Cro_2}\sum_{\nu=1}^{2}\Delta G^{Y}_{O_{X^{\nu\nu+1}}}\Gamma^{Y}_{O_{X^\nu}}(i)\Gamma^{Y}_{O_{X^{\nu+1}}}(i) + \sum_{X=R,L}\Delta G^{Cro_2}_{O_{X123}}\Gamma^{Cro_2}_{O_{X^1}}(i)\Gamma^{Cro_2}_{O_{X^2}}(i)\Gamma^{Cro_2}_{O_{X^3}}(i) + \sum_{X=RM,R,L}\Delta G^{RNAP}_{P_X}\Gamma^{RNAP}_{P_X}(i) + \sum_{\nu=1}^{3}\Delta G_{RL}\Gamma^{CI_2}_{O_{R^\nu}}(i)\Gamma^{CI_2}_{O_{L^\nu}}(i), \quad (1)$$

where

$$\Gamma^{Y}_{X}(i) = \begin{cases} 1, & \textit{if molecule Y is bound to site X} \\ 0, & \textit{otherwise} \end{cases}.$$

The terms $\Delta G^{RNAP}_{P_X}$ (X = RM, R, L) represent the binding energy of a RNAP molecule bound to site P_X, the terms $\Delta G^{Y}_{O_{X^\nu}}$ (X = R, L) represent the binding energy of molecule Y to site O_{X^ν}, the terms $\Delta G^{Y}_{O^{\nu\nu+1}}$ represent the interaction energy between two Y molecules bound to sites O_{X^ν} and $O_{X^{\nu+1}}$, and the terms $\Delta G^{Cro_2}_{O_{X123}}$ represent the interaction energy between three Cro_2 molecules bound to O_X1, O_X2, and O_X3. All of these individual binding and interaction energies have been measured elsewhere and are given in Appendix A. To our knowledge, the interaction energy between CI_2's bound to operators O_R and O_L has not yet been measured. The present model assumes that whenever there is one CI_2 bound to $O_R\nu$ and a second CI_2 is bound to $O_L\nu$, they interact with an energy ΔG_{RL} whose value is also estimated in Appendix A.

Following the same technique used by Ackers et al. (l982) and Shea and Ackers (1985), under the assumption of thermodynamic equilibrium, the probability of every one of the 1200 binding states can be calculated from

$$P_i = \frac{\exp(-E_i/RT)[CI_2]^{\alpha_i}[Cro_2]^{\beta_i}[RNAP]^{\gamma_i}}{Z}. \quad (2)$$

In Eq. 2, P_i and E_i are the probability and the energy of the i-th binding state, respectively. R is the ideal gas constant and T is the absolute temperature. Here we take $T = 37°C$ so $RT \simeq 0.617$ kcal/mol (Ackers et al., 1982; Shea and Ackers, 1985). The partition function Z is given by

$$Z = \sum_i \exp(-E_i/RT)[CI_2]^{\alpha_i}[Cro_2]^{\beta_i}[RNAP]^{\gamma_i}. \quad (3)$$

Finally, $[CI_2]$, $[Cro_2]$, and $[RNAP]$ are, respectively, the concentration of CI_2, Cro_2, and RNA polymerase molecules,

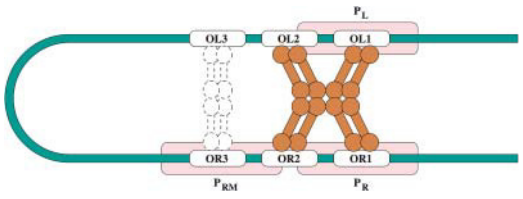

FIGURE 2 Proposed interaction between CI_2s bound at O_R and O_L.

whereas α_i, β_i, and γ_i are, respectively, the number of CI_2, Cro_2, and RNA polymerase molecules bound to the operator-promoter complex in the i-th state.

Note that the thermodynamic equilibrium assumption does not mean that the probabilities remain constant in time. Rather, it means that the probabilities considered are those that would be attained by the real system if it would have enough time to reach the state of thermodynamic equilibrium, given the concentrations $[CI_2]$, $[Cro_2]$, and $[RNAP]$. If these concentrations are time dependent, the probabilities given under the thermodynamic equilibrium assumption will change accordingly. If the chemical processes involving association and dissociation of CI_2 and Cro_2, as well as RNA polymerase molecules to the right operator-promoter complex, take place rapidly (relative to the temporal changes of the concentrations $[CI_2]$, $[Cro_2]$, and $[RNAP]$), the thermodynamic equilibrium assumption is appropriate.

The probability f_R for P_R to be bound by a polymerase can be calculated by adding the probability of all compatible states, i.e., all the states in which a polymerase is bound to P_R while O_R1 and O_R2 are free, independent of the states of O_R3, P_{RM}, O_L1, O_L2, O_L3, and P_L. Similarly, the probability f^q_{RM} for a polymerase to be bound to P_{RM} with a CI_2 bound to O_R2 can be calculated by adding the probability of all the binding states in which O_R3 is free, a polymerase is bound to P_{RM}, and a CI_2 is bound to O_R2, no matter what the states of O_R1, P_R, O_L1, O_L2, O_L3, and P_L are. Finally, the probability f^s_{RM} for a polymerase to be bound to P_{RM} without a CI_2 bound to O_R2 is calculated by adding the probability of all the states in which O_R3 is free, a polymerase is bound to P_{RM}, and O_R2 is either free or bound by a Cro_2 independent of the states of O_R1, P_R, O_L1, O_L2, O_L3, and P_L.

The rate at which RNA polymerase molecules start transcription of the genes *cro* and *cI* can be written as $k_{cro}f_R[O_R]$ and $(k^q_{cI}f^q_{RM}+k^s_{cI}f^s_{RM})[O_R]$, respectively (Ackers et al., 1982; Shea and Ackers, 1985). k_{cro} is the transcription initiation rate constant of promoter P_R, whereas k^q_{cI} and k^s_{cI} are the transcription initiation rate constants of promoter P_{RM} when O_R2 is bound by or free from a CI_2 molecule, respectively. O_R is the right operator concentration.

Let $[M_{cI}]$ and $[M_{cro}]$ be the concentration of *cI* and *cro* mRNA molecules, respectively. Let $[CI_T]$ and $[Cro_T]$, respectively, denote the total concentration of CI and Cro monomers. These concentrations are calculated by adding the free monomer plus twice the dimer concentrations. Thus, from the considerations in the previous paragraphs, we propose the following equations to model the dynamic evolution of $[M_{cI}]$, $[M_{cro}]$, $[CI_T]$, and $[Cro_T]$:

$$\frac{d[M_{cI}]}{dt} = k^q_{cI}[O_R]f^q_{RM}([CI_2]_{\tau_M}, [CI_2]_{\tau_M}) + k^s_{cI}[O_R]f^s_{RM}([CI_2]_{\tau_M}, [Cro_2]_{\tau_M}) - (\gamma_M + \mu)[M_{cI}], \quad (4)$$

$$\frac{d[M_{cro}]}{dt} = k_{cro}[O_R]f_R([CI_2]_{\tau_M}) - (\gamma_M + \mu)[M_{cro}], \quad (5)$$

$$\frac{d[CI_T]}{dt} = \upsilon_{cI}[M_{cI}]_{\tau_{cI}} - (\gamma_{cI} + \mu)[CI_T], \quad (6)$$

and

$$\frac{d[Cro_T]}{dt} = \upsilon_{cro}[M_{cro}]_{\tau_{cro}} - (\gamma_{cro} + \mu)[Cro_T]. \quad (7)$$

The meaning of all parameters appearing for the first time in these equations is as follows: γ_M is the rate of mRNA degradation; γ_{cro} is the rate of Cro_T degradation; γ_{cI} is the rate of CI_T degradation; τ_M is time required after transcription initiation to have a mRNA ready to be bound by a ribosome; τ_{cI} is the time it takes to translate a monomer CI; τ_{cro} is the time it takes to translate a monomer Cro; υ_{cI} is the rate of *cI* translation initiation; and υ_{cro} is the rate of *cro* translation initiation. The notation X_τ means $X_\tau \equiv X(t-\tau)$.

The dimer concentrations ($[CI_2]$ and $[Cro_2]$) can be calculated in terms of the total monomer concentrations ($[CI_T]$ and $[Cro_T]$) if we make a quasi-steady-state assumption for the dimerization reactions (see Appendix B):

$$[CI_2] = \frac{1}{2}[CI_T] - \frac{K^{cI}_D}{8}\left[\sqrt{1 + 8\frac{[CI_T]}{K^{cI}_D}} - 1\right], \quad (8)$$

and

$$[Cro_2] = \frac{1}{2}[Cro_T] - \frac{K^{cro}_D}{8}\left[\sqrt{1 + 8\frac{[Cro_T]}{K^{cro}_D}} - 1\right], \quad (9)$$

where K^{cI}_D and K^{cro}_D, respectively, denote the CI and Cro dimerization dissociation constants.

The values of all of the parameters in Eq. 4–9 are estimated in Appendix A and tabulated in Table 1.

NUMBER AND LOCATION OF THE STEADY STATES

The model given by Eq. 4–9 reaches a steady state whenever $d[M_{cI}]/dt = 0$, $d[M_{cro}]/dt = 0$, $d[CI_T]/dt = 0$, and $d[Cro_T]/dt = 0$. Given that, in the steady state, all of the delayed variables attain their steady-state value, the time delays τ_M, τ_{cI}, and τ_{cro} may be ignored. It can be shown after a little

TABLE 1 Estimated values for the parameters in Eq. 4–9

$\mu \simeq 2.0 \times 10^{-2}$ min^{-1}	$k_{cro} \simeq 2.76$ min^{-1}
$k^q_{cI} \simeq 4.29$ min^{-1}	$k^s_{cI} \simeq 0.35 \times$ min^{-1}
$\gamma_M \simeq 0.12$ min^{-1}	$\gamma_{cI} \simeq 0.0$ min^{-1}
$\gamma_{cro} \simeq 1.6 \times 10^{-2}$ min^{-1}	$\upsilon_{cI} \simeq 0.09$ min^{-1}
$\upsilon_{cro} \simeq 3.2$ min^{-1}	$\tau_{cI} \simeq 0.24$ min
$\tau_{cro} \simeq 6.6 \times 10^{-2}$ min	$\tau_M \simeq 5.1 \times 10^{-3}$ min
$K^{cI}_D \simeq 5.56 \times 10^{-3}\,\mu$M	$K^{cro}_D \simeq 3.26 \times 10^{-1}\,\mu$M
$[O_R] \simeq 5.0 \times 10^{-3}\,\mu$M	[mRNAP] $\simeq 3.0\,\mu$M
$\Delta G_{RL} \simeq -3.1$ kcal/mol	

algebra that the CI_T and Cro_T steady-state values satisfy the following equations:

$$\Phi([CI_T],[Cro_T],\gamma_{cI}) = 0, \tag{10}$$

and

$$\Theta([CI_T],[Cro_T]) = 0, \tag{11}$$

where

$$\Phi([CI_T],[Cro_T],\gamma_{cI}) = \frac{\upsilon_{cI}}{\gamma_M+\mu}[O_R](k^q_{cI}f^q_{RM} + k^s_{cI}f^s_{RM}) - (\gamma_{cI}+\mu)[CI_T], \tag{12}$$

and

$$\Theta([CI_T],[Cro_T]) = \frac{\upsilon_{cro}}{\gamma_M+\mu}[O_R]k_{cro}f_R - (\gamma_{cro}+\mu)[Cro_T]. \tag{13}$$

The equation $\Phi([CI_T],[Cro_T],\gamma_{cI}) = 0$ determines a family of curves in the $([CI_T],[Cro_T])$ space (one for every value of γ_{cI}), whereas the equation $\Theta([CI_T],[Cro_T]) = 0$ determines one single curve in the same space. For a given value of γ_{cI}, the points where the curves $\Phi = 0$ and $\Theta = 0$ intersect correspond to the steady states of the system.

The curve $\Theta = 0$ is shown in Fig. 3 in the $[Cro_T]$ vs. $[CI_T]$ phase space, along with $\Phi = 0$ curves for various values of γ_{cI}. For the normal lysogenic value $\gamma_{cI} \simeq 0.0\ \text{min}^{-1}$ (see Table 1), both curves intersect at only one point implying that for this value of γ_{cI} there is only one steady state. This steady state is stable (this point is discussed below in more detail) and corresponds to the lysogenic steady state. Nevertheless, this behavior is at the verge of a bifurcation because a slight increment of γ_{cI} makes the curve $\Phi = 0$ tangentially intersect the curve $\Theta = 0$. At this point, two more steady states appear via a saddle node bifurcation. One of these steady states is stable and corresponds to the lytic state (see below for more detail), whereas the other is a saddle node. With further increases in γ_{cI}, the lytic steady state separates from the saddle node, and the saddle node approaches the lysogenic steady state. When γ_{cI} reaches a value of $\sim 0.35\ \text{min}^{-1}$, the saddle node and the lysogenic state collide and annihilate through a reverse saddle node bifurcation.

NUMERICAL TEST OF THE STEADY STATES' STABILITY PROPERTIES

Consider the system of time-delay differential equations given by Eq. 4–7. In Table 1, it is clear that the time delay τ_M is one order of magnitude smaller than τ_{cI} and two orders of magnitude smaller than τ_{cro}. This observation allows us to slightly simplify the model by ignoring the time delay τ_M wherever it appears. After this simplification, the system of equations was numerically solved by means of the fourth-order Runge-Kutta algorithm (adapted to account for the time delays), implemented in FORTRAN.

Projections of the phase space trajectories onto the $([CI_T],[Cro_T])$ space are shown in Fig. 4 for various values of γ_{cI}. The curves in this figure exemplify a large amount of numerical experiments that we performed to test the steady states' stability properties. These properties can be described as follows: for $\gamma_{cI} = 0.0\ \text{min}^{-1}$ the system has one single globally stable steady state corresponding to lysogeny (Fig. 4 *A*). A slight increment of γ_{cI} beyond this value produces two more steady states via a saddle node bifurcation. One of these is stable and corresponds to lysis whereas the other is an unstable saddle node (Fig. 4 *B*). This bistable behavior is maintained with further increments of γ_{cI} until about $\gamma_{cI} \simeq 0.35\ \text{min}^{-1}$, when the saddle node and the lysogenic steady state collide annihilating each other by means of a reverse saddle node bifurcation. For γ_{cI}'s larger than $0.35\ \text{min}^{-1}$

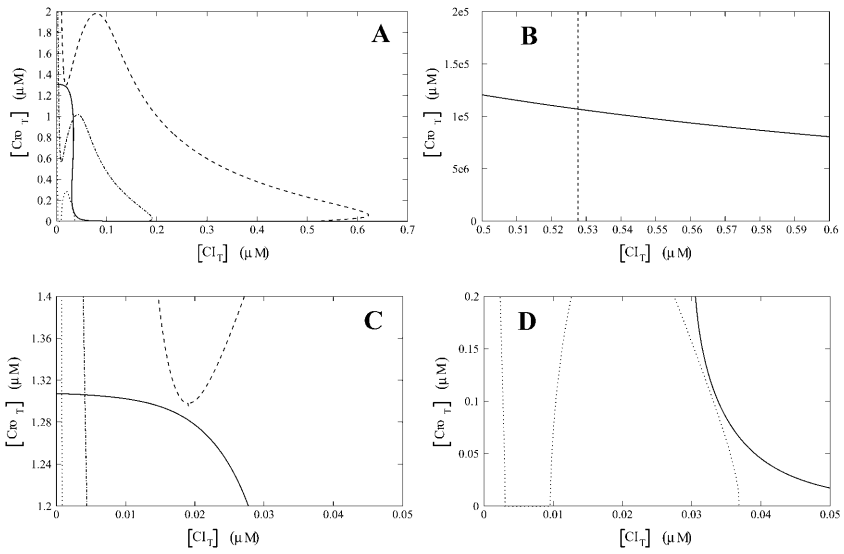

FIGURE 3 Plots in the $[Cro_T]$ vs. $[CI_T]$ plane of the $\Theta = 0$ curve (*solid line*) and of the $\Phi = 0$ curves for various values of γ_{cI}: the dashed line corresponds to $\gamma_{cI} = 0.0\ \text{min}^{-1}$, the dot-dashed line corresponds to $\gamma_{cI} = 0.05\ \text{min}^{-1}$, and the dotted curve corresponds to $\gamma_{cI} = 0.35\ \text{min}^{-1}$. Intersections between the $\Theta = 0$ and $\Phi = 0$ plots locate the system steady states. The whole curves are shown in *A*. In *B*, the lysogenic steady state corresponding to $\gamma_{cI} = 0$ is shown, whereas in *C* and *D* we show zooms of the regions where the bifurcations take place. All these curves were numerically calculated with the aid of Octave's algorithm "fsolve."

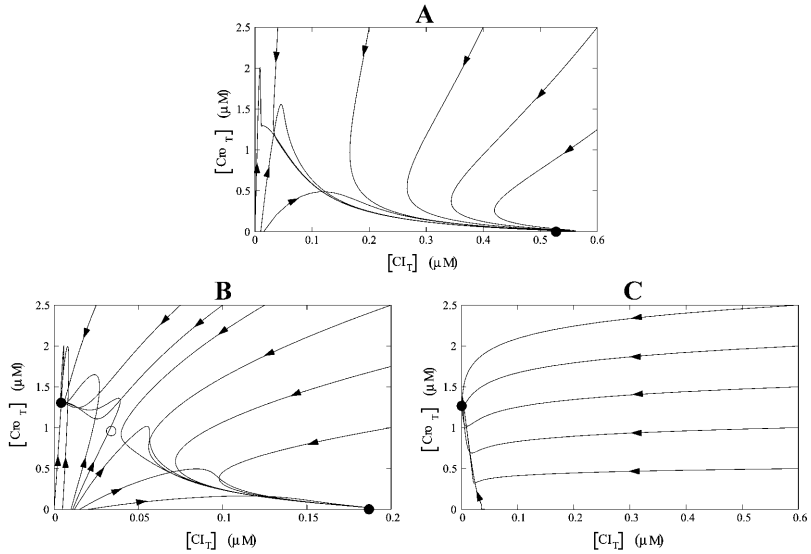

FIGURE 4 Projections onto the ($[CI_T]$,$[Cro_T]$) space of the phase space trajectories (derived from the numerical solutions of the system time-delay differential equations, for various initial conditions) of the phage λ switch model for different values of γ_{cI}: (*A*) $\gamma_{cI} = 0.0\ \text{min}^{-1}$, (*B*) $\gamma_{cI} = 0.05\ \text{min}^{-1}$, and (*C*) $\gamma_{cI} = 0.35\ \text{min}^{-1}$. Note that the tangled appearance of the trajectories in *A* and *B* are due to the projection from a four-dimensional phase space into the plane. Stable steady states are indicated with filled circles, whereas unstable steady states, if any, are indicated with empty circles.

the system has one single globally stable lytic steady state (Fig. 4 *C*).

We numerically solved the model equations by changing the value of parameters other than γ_{cI} to test the robustness of our results. We found that of all the parameters, the model is particularly sensitive to changes in ΔG_{RL}. Indeed, for absolute values of ΔG_{RL}'s smaller than 3.1 kcal/mol the system shows a bistable behavior even for $\gamma_{cI} = 0.0\ \text{min}^{-1}$. When the absolute value of ΔG_{RL} is increased beyond 3.1 kcal/mol, the system has one single steady state (corresponding to lysogeny) for $\gamma_{cI} = 0.0\ \text{min}^{-1}$, and the values of γ_{cI} at which the bifurcations take place increase. This behavior is pictured as a bifurcation diagram in Fig. 5. The above described results indicate that cooperativity between the right and left operator regions plays a very important role in the stability of the lysogeny steady state. Moreover, they also highlight the necessity of detailed experiments to clarify the nature of the interaction between CI dimers bound to the left and right operator regions.

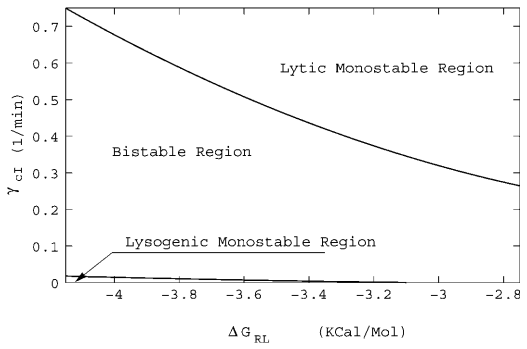

FIGURE 5 Bifurcation diagram in the (ΔG_{RL}, γ_{cI}) parameter space. Three different qualitative dynamic behaviors, which correspond to the three regions illustrated in the bifurcation diagram, can be observed: either the system has one single stable steady state corresponding to lysogeny, it has only one stable steady state corresponding to lysis, or it has three steady states, two of them being stable (the lysogenic and lytic states) and the other being a saddle node. The boundaries between the three regions identify the values of ΔG_{RL} and γ_{cI} at which the bifurcations take place.

Some of the estimated parameters were obtained by averaging previously reported values. In some cases, the relative errors are higher than 30%. This is in particular the case with $k_{cI}^{s} \in [0.3, 0.41]\text{min}^{-1}$ and $k_{cI}^{q} \in [3.42, 5.16]\text{min}^{-1}$. To test how this variability affects the system dynamic behavior we redraw the plots of Fig. 3 (which illustrate the number and location of the system's steady states for different values of γ_{cI}) using the extreme values of the P_{RM} transcription initiation rates k_{cI}^{s} and k_{cI}^{q}. These plots are presented in Fig. 6. There, notice that with the lowest k_{cI}^{s} and k_{cI}^{q} values, the system shows bistability even for $\gamma_{cI} = 0\ \text{min}^{-1}$. Moreover, the γ_{cI} value at which the lysogenous steady state and the saddle node collide and annihilate decreases. A comparison with the bifurcation diagram of Fig. 5 reveals that the only effect of decreasing the values of k_{cI}^{s} and k_{cI}^{q} is to slightly displace the bifurcation curves of Fig. 5 to the left along the ΔG_{RL} axis. Similarly, increasing the k_{cI}^{s} and k_{cI}^{q} values has the single effect of slightly displacing the bifurcation curves to the right. Thus, we conclude that changes of parameters k_{cI}^{s} and k_{cI}^{q} even larger than 30% do not alter the overall qualitative dynamic behavior of the system.

CONCLUSIONS

Our results provide a possible answer to the question of why the lysogenic steady state is so stable. Namely, from our model and analysis the phage λ switch has only one steady state under normal conditions. Moreover, based on our numerical results the lysogeny steady state appears to be globally stable. This is in agreement with the fact that the lysogenic state is even more stable than the genome itself. Only that fraction of mutations that typically increase the CI degradation rate can cause some lysogens to become lytic.

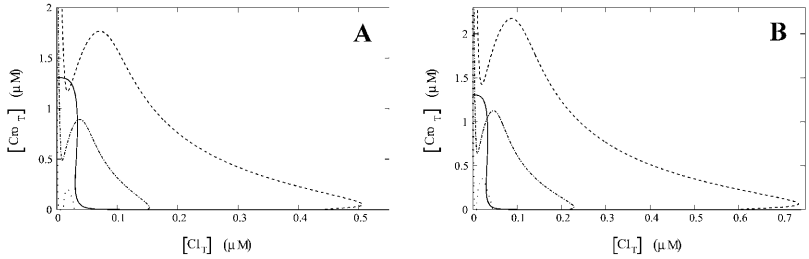

FIGURE 6 Plots in the $[Cro_T]$ vs. $[CI_T]$ plane of the $\Theta = 0$ curve (*solid line*) and of the $\Phi = 0$ curves for various values of γ_{cI}: the dashed line corresponds to $\gamma_{cI} = 0.0\ min^{-1}$, the dot-dashed line corresponds to $\gamma_{cI} = 0.05\ min^{-1}$, and the dotted curve corresponds to $\gamma_{cI} = 0.35\ min^{-1}$. Intersections between the $\Theta = 0$ and $\Phi = 0$ plots locate the system steady states. The plots in *A* and *B* were calculated, respectively, with the smallest and largest values of k_{cI}^{s} and k_{cI}^{q} reported in the literature.

Conversely, if after being irradiated with UV light the activated RecA proteins cleave CI monomers at a rate $>0.35\ min^{-1}$, all of the infected bacteria will go into lysis. This will happen because lysis will be the only available steady state, which is globally stable under this condition. Thus, by taking into account the cooperativity between CI_2's bound at the O_R and O_L operators, it is possible to explain the astonishingly high stability of the phage λ lysogenic state, as well as the almost perfect efficiency of the switch.

The estimated energy of interaction between CI_2's bound to the left and right operators (ΔG_{RL}), relies on an assumed interaction that has not been experimentally demonstrated. Nevertheless, we believe our model is robust in this respect based on the fact that the value we estimate for ΔG_{RL} is similar to the measured interaction energy between CI_2's bound to adjacent O_R sites (see Appendix A). Furthermore, our assumption can be tested experimentally.

In this work, we predict bistable behavior (between the lysogenic and lytic states) for CI degradation rates (γ_{cI}) larger than 0.0 but smaller than $0.35\ min^{-1}$. To test this prediction, mutant phage λ strains in which CI is not as stable as it is in the wild type would be useful. If for such mutant strains γ_{cI} is large enough to induce bistable behavior, a rate of lysogen loss of the same order of magnitude as that predicted by Arkin et al. (1998) should be observed, instead of the (orders of magnitude smaller) wild-type loss rate. Other possible tests of the model would involve mutant *E. coli* strains, in which the activated RecA proteins fail to cleave CI at a rate high enough to induce one single lytic stable steady state. Then, the system would still be in the bistable region, and some of the lysogens would always survive after having been irradiated with UV light.

The dynamic influence of the thermodynamic equilibrium approximation, on which this and other models rely, should be analyzed. In our particular case, this approximation is equivalent to a quasi-steady-state assumption for the chemical reactions by means of which CI_2, Cro_2, and RNA polymerase molecules bind to, and detach from, the promoter-operator regions. Its validity relies upon the assumption that those chemical reactions are rapid, relative to the transcription and translation processes. In other words, the feasibility of a thermodynamic equilibrium (or a quasi-steady-state) assumption is a question of having phenomena with orders-of-magnitude different characteristic times. In our opinion, although it is not plausible that a phenomenological model based on a thermodynamic equilibrium approximation will generally work for living biological systems, it seems to work well here because the required difference in characteristic times is fulfilled.

The model here presented does not allow us to make quantitative predictions concerning the lysogen loss and survival rates of wild-type and mutant λ strains, under different experimental conditions. To make them, the fluctuations inherent to molecular systems should be accounted for in a stochastic model.

Finally, we call attention to the fact that the model is highly sensitive to changes in the parameter ΔG_{RL}. This indicates that the interaction between CI dimers bound to the left and right operator regions plays an important role in the stability of the lysogeny state. However, it also highlights the necessity of detailed experiments concerning this interaction to validate our results.

APPENDIX A: PARAMETER ESTIMATION

The CI_2 and Cro_2 binding energies to O_R1, O_R2, and O_R3, the interaction energy between CI_2's or Cro_2's bound to adjacent sites, and the RNA polymerase binding energy to P_R and P_{RM} have been measured elsewhere. The most recent, and presumably most accurate, values are reported by Darling et al. (2000b) and tabulated in Table 2.

TABLE 2 Binding energies of Cl_2 and Cro_2 to O_R1, O_R2, and O_R3 ($\Delta G^{Cl_2}_{O_Ri}$ and $\Delta G^{Cro_2}_{O_Ri}$, $i = 1,2,3$), interaction energies between adjacent Cl_2's or Cro_2's ($\Delta G^{Cl_2}_{O_Rij}$, $\Delta G^{Cro_2}_{O_Rij}$, and $\Delta G^{Cro_2}_{O_R123}$, $i < j$) (in this case the dimer-operator binding energies are not considered), and RNA polymerase (RNAP) binding energies to P_R and P_{RM} ($\Delta G^{RNAP}_{P_R}$ and $\Delta G^{RNAP}_{P_{RM}}$)

$\Delta G^{CI_2}_{O_R1} \simeq -12.5\ kcal/mol$
$\Delta G^{CI_2}_{O_R2} \simeq -10.5\ kcal/mol$
$\Delta G^{CI_2}_{O_R3} \simeq -9.5\ kcal/mol$
$\Delta G^{CI_2}_{O_R12} \simeq -2.7\ kcal/mol$
$\Delta G^{CI_2}_{O_R23} \simeq -2.9\ kcal/mol$
$\Delta G^{Cro_2}_{O_R1} \simeq -12.0\ kcal/mol$
$\Delta G^{Cro_2}_{O_R2} \simeq -10.8\ kcal/mol$
$\Delta G^{Cro_2}_{O_R3} \simeq -13.4\ kcal/mol$
$\Delta G^{Cro_2}_{O_R12} \simeq -1.0\ kcal/mol$
$\Delta G^{Cro_2}_{O_R23} \simeq -0.6\ kcal/mol$
$\Delta G^{Cro_2}_{O_R123} \simeq -0.9\ kcal/mol$
$\Delta G^{RNAP}_{P_R} \simeq -12.5\ kcal/mol$
$\Delta G^{RNAP}_{P_{RM}} \simeq 11.5\ kcal/mol$

The CI_2 and Cro_2 single-site binding energies at O_L are reported by Aurell and Sneppen (2002). However, these energies were measured before the cooperativity between Cro_2's bound to adjacent sites was discovered. Cro_2 single-site binding energies at O_R reported before and after cooperativity was discovered are very different. This is not the case with CI_2 (Darling et al., 2000b). Moreover, Cro_2 single-site binding energies at O_R, that also ignore cooperativity, are very similar to those of O_L (Aurell et al., 2002). From this, we take the CI_2 single-site binding energies reported by Aurell and Sneppen (2002), but for the CI_2 cooperativity and Cro_2 single-site binding and cooperativity energies at O_L we assume that they are equal to those of O_R. Giladi et al. (1990) measured the association constant of the polymerase-P_L closed complex formation. They report a value of $K_B \simeq 8.94 \times 10^7$ mol^{-1}. From this and taking $RT \simeq 0.617$ kcal/mol, we can estimate the RNA polymerase-P_L binding energy to be $\Delta G_{PL}^{RNAP} = -RT\ln(K_B) \simeq -11.3$ kcal/mol. These energies are tabulated in Table 3.

The value of the probabilities f_R, f_{RM}^q, and f_{RM}^s can be calculated for every value of $[CI_2]$ and $[Cro_2]$ from the energy values tabulated in Tables 2 and 3, as well as from the energy ΔG_{RL} and the RNA polymerase concentration $[RNAP]$ (the last two parameters are estimated below). We also need estimates for the right operator concentration $[O_R]$, the growth rate μ, the degradation rates γ_M, γ_{cI}, and γ_{cro}, the transcription initiation rates k_{cI}^q, k_{cI}^s, and k_{cro}, and for the translation initiation rates υ_{cI} and υ_{cro}.

Growth rate

Reinitz and Vaisnys (1990) and Little et al. (1999) performed experiments on the shift of the phage λ switch from the lysogeny to the lytic state. In these experiments, they employ a bacterial generation time of ~34 min. For the purpose of the present work, we will consider the same generation time, which corresponds to a growth rate of $\mu \simeq 2.0 \times 10^{-2}$ min^{-1}.

E. coli volume

E. coli are rodlike bacteria 3–5 μm long and 0.5 μm in diameter, so they have a volume in the range from 6.0×10^{-16} L to 9.8×10^{-16} L. We considered a mean volume of 8.0×10^{-16} L.

RNA polymerase concentration [*RNAP*]

According to Bremer and Dennis (1996), there are ~1,500 RNA active polymerase molecules per cell in *E. coli* bacterial cultures growing at the rate μ as estimated above. This leads to a concentration $[RNAP] \simeq 3.0$ μM.

TABLE 3 Energies of Cl_2 and Cro_2 binding to O_L1, O_L2, and O_L3 ($\Delta G_{O_Li}^{Cl_2}$ and $\Delta G_{O_Li}^{Cro_2}$, $i = 1,2,3$), interaction energies between adjacent Cl_2's or Cro_2's ($\Delta G_{O_Lji}^{Cl_2}$, $\Delta G_{O_Lji}^{Cro_2}$, and $\Delta G_{O_L123}^{Cro_2}$, $i < j$) (in this case the dimer-operator binding energies are not considered), and energies of RNA polymerase (RNAP) binding to P_L ($\Delta G_{P_L}^{RNAP}$)

$\Delta G_{O_L1}^{CI_2} \simeq -11.5$ kcal/mol
$\Delta G_{O_L2}^{CI_2} \simeq -9.7$ kcal/mol
$\Delta G_{O_L3}^{CI_2} \simeq -9.7$ kcal/mol
$\Delta G_{O_L12}^{CI_2} \simeq -2.7$ kcal/mol
$\Delta G_{O_L23}^{CI_2} \simeq -2.9$ kcal/mol
$\Delta G_{O_L1}^{Cro_2} \simeq -12.0$ kcal/mol
$\Delta G_{O_L2}^{Cro_2} \simeq -10.8$ kcal/mol
$\Delta G_{O_L3}^{Cro_2} \simeq -13.4$ kcal/mol
$\Delta G_{O_L12}^{Cro_2} \simeq -1.0$ kcal/mol
$\Delta G_{O_L23}^{Cro_2} \simeq -0.6$ kcal/mol
$\Delta G_{O_L123}^{Cro_2} \simeq -0.9$ kcal/mol
$\Delta G_{P_L}^{RNAP} \simeq -11.3$ kcal/mol

Right operator concentration [O_R]

According to Bremer and Dennis (1996), there are ~2.5 genome equivalents per average *E. coli* cell at the growth rate determined by μ. Assuming one operator O_R per genome equivalent, the right operator concentration can be estimated as $[O_R] \simeq 5.0 \times 10^{-3}$ μM.

Average lysogenic CI_T concentration

According to Ptashne (1986), there are between 200 and 350 CI molecules per cell (in monomer units) in lysogenic bacteria. Here, we take the mean number 275, which corresponds to a concentration of $[\overline{CI}]_{lysogeny} \simeq 0.55$ μM.

P_R transcription initiation rate k_{cro}

Hawley et al. (1985) and Fong et al. (l994) report measurements of the closed-to-open complex isomerization rate at the P_R operator k_{cro}. The values they report are respectively: $k_{cro} \simeq 5.0 \times 10^{-2}$ s^{-1} and $k_{cro} \simeq 4.12 \times 10^{-2}$ s^{-1}. We take the mean value $k_{cro} \simeq 4.6 \times 10^{-2}$ s^{-1} $\simeq 2.76$ min^{-1}.

P_{RM} transcription initiation rates k_{cI}^q and k_{cI}^s

Hwang et al. (1988) and Li et al. (1997) report measurements of the closed-to-open complex isomerization rate at the P_{RM} operator. According to Hwang et al. (1988), this rate in the absence of CI_2 repressor is around $k_{cI}^s \simeq 0.68 \times 10^{-2}$ s^{-1} and $k_{cI}^q \simeq 5.7 \times 10^{-2}$ s^{-1} in the presence of CI_2 repressor. Li et al. (1997) report the following values: $k_{cI}^s \simeq 0.5 \times 10^{-2}$ s^{-1} and $k_{cI}^q \simeq 8.6 \times 10^{-2}$ s^{-1}. We consider here the mean values: $k_{cI}^s \simeq 0.59 \times 10^{-2}$ s^{-1} $\simeq 0.35$ min^{-1} and $k_{cI}^q \simeq 7.15 \times 10^{-2}$ s^{-1} $\simeq 4.29$ min^{-1}.

mRNA degradation rate γ_M

Court et al. (1980) performed experiments to measure the half-life of P_L transcripts. They report $\tau_{1/2} \simeq 6$ min, and assert that the half-lives of the P_R and P_{RM} transcripts are similar. From this, the mRNA degradation rate can be estimated to be $\gamma_M = \ln 2/\tau_{1/2} \simeq 0.12$ min^{-1}.

CI_T degradation rate γ_{cI}

Following Hawley et al. (l985), Reinitz and Vaisnys (1990), Aurell et al. (2002), and Aurell and Sneppen (2002), we ignore the degradation rate of CI_T because it is very small compared with other rates in the model, e.g., the growth rate μ. Therefore, we take $\gamma_{cI} = 0$.

Cro_T degradation rate γ_{cro}

Pakula et al. (1986) measured a Cro half-life in vivo of ~2600 s $\simeq 43.3$ min. From this, $\gamma_{cro} \simeq 1.6 \times 10^{-2}$ min^{-1}.

cI translation initiation rate υ_{cI}

Under normal conditions, the system of time-delay differential equations (Eq. 4–7) model has one single stable steady state corresponding to lysogeny. In this lysogenic state, P_R is very tightly repressed whereas P_{RM} is repressed only ≈20% (Dodd et al., 2001; Meyer et al., 1980). Because $k_{cI}^q > k_{cI}^s$, the maximum activity of the promoter P_{RM} corresponds to $f_{RM}^q = 1$ and $f_{RM}^s = 0$ and is given by $k_{cI}^q[O_R]$. Thus, the normalized activity of the promoter P_{RM} in the lysogenic state is $f_{RM}^q + k_{cI}^s/k_{cI}^q f_{RM}^s = 0.8$, with which the dynamic equation for $[M_{cI}]$ becomes

$$\frac{d[M_{cI}]}{dt} = 0.8k_{cI}^{q} - (\gamma_M + \mu)[M_{cI}].$$

By solving for the *cI* translation initiation rate υ_{cI} from this last equation and the dynamic equation for $[M_{cro}]$, and taking into account that the concentration of all chemical species is constant in a steady state ($d[M_{cI}]/dt = 0$ and $d[CI_T]/dt = 0$), we obtain

$$\upsilon_{cI} = \frac{(\gamma_{cI} + \mu)(\gamma_M + \mu)}{0.8k_{cI}^{q}} \frac{[CI_{lysogeny}]}{[O_R]} \simeq 0.09\,\mathrm{min}^{-1}.$$

cro translation initiation rate υ_{cro}

Aurell et al. (2002) estimate that, when translated, a *cro* transcript produces 51% of the polypeptides an ideal *lac*Z transcript produces. From this and taking into account that ribosomes load onto *lac*Z transcripts at 3.2 s = 5.33 $\times 10^{-2}$ min intervals (Kennell and Riezman, 1977), that the *lac*Z transcript half-life is ~2 min (Leive and Kollin, 1967), and that the *cro* transcript half-life is of the order of 6 min (Court et al., 1980), the *cro* translation initiation rate can be estimated as $\upsilon_{cro} \simeq (0.51 \times 2\ \mathrm{min}) / (6\ \mathrm{min} \times 5.33 \times 10^{-2}\ \mathrm{min}) \simeq 3.2\ \mathrm{min}^{-1}$.

The time delays due to *cI* and *cro* translation τ_{cI} and τ_{cro}

CI and Cro are proteins that are 267 and 66 amino-acid-long, respectively. This means that gene *cI* is 711 basepairs long, whereas *cro* gene is 198 basepairs long. From this and taking into account that, according to Bremer and Dennis (1996), the mRNA chain elongation rate is ~50 nucleotide/s, the time it takes for genes *cI* and *cro* to be translated is $\tau_{cI} \simeq 0.24$ min and $\tau_{cro} \simeq 6.6 \times 10^{-2}$ min, respectively.

The time delay due to transcription τ_M

Once a RNA polymerase has transcribed a mRNA chain long enough for a ribosome to bind to it, translation can start. According to Draper (1996), efficient mRNA's can initiate translation every 3 s. From this and the fact that the mRNA chain elongation rate is of the order of 50 nucleotide/s (Bremer and Dennis, 1996), <150 nucleotides are required for a ribosome to bind a mRNA and start translation. Furthermore, the DNA chain elongation rate is at least 490 nucleotide/s (Bremer and Dennis, 1996). Thus it takes <0.31 s after transcription initiation to have a mRNA ready for translation initiation. i. e., $\tau_M \simeq 5.1 \times 10^{-3}$ min.

The CI and Cro dimerization dissociation constants K_D^{cI} and K_D^{cro}

Burz et al. (1994) measured the CI dimerization dissociation constant obtaining $K_D^{cI} \simeq 5.56 \times 10^{-3}\ \mu$M. The Cro dimerization dissociation constant was measured by Darling et al. (2000a) to give $K_D^{cro} \simeq 3.26 \times 10^{-1}\ \mu$M.

Interaction energy between CI_2 dimers bound to O_R and O_L, ΔG_{RL}

According to Meyer et al. (1980) and Dodd et al. (2001), P_R is very tightly repressed whereas P_{RM} is repressed only ≃20% in the lysogenic state. From this, the P_{RM} transcription initiation rate $k_{cI}^{q}[O_R]f_{RM}^{q} + k_{cI}^{s}[O_R]f_{RM}^{s}$ should be 80% of the maximum transcription initiation rate $k_{cI}^{q}[O_R]$. That is, $f_{RM}^{q} + k_{cI}^{s}/k_{cI}^{q} f_{RM}^{s} = 0.8$. After substitution of the steady state $[CI_T] \simeq 0.55\ \mu$M and $[Cro_T] \simeq 0.0\ \mu$M values this becomes a nonlinear algebraic equation of ΔG_{RL} which, when solved with the aid of Octave's algorithm "fsolve" gives:

$$\Delta G_{RL} \simeq -3.1\,\mathrm{kcal/mol}.$$

APPENDIX B: DIMERIZATION KINETICS

Consider the following chemical reaction:

$$2a \underset{k_-}{\overset{k_+}{\longleftrightarrow}} a_2.$$

In this equation, a_2 represents a dimer of chemical species a, and k_+ and k_- are the forward and backward reaction rates, respectively.

In a state of chemical equilibrium the following relation is satisfied,

$$[a]^2 = K_D[a_2],$$

where $K_D = k_-/k_+$ is the so-called dissociation constant and $[x]$ represents the concentration of species x. Let $[a_T]$ be the total monomer concentration:

$$[a_T] = [a] + 2[a_2].$$

The last two equations constitute a complete set of equations for the variables $[a]$ and $[a_2]$. By solving for $[a_2]$ we obtain the following expression for the dimer concentration in terms of a_T and K_D,

$$[a_2] = \frac{[a_T]}{2} = \frac{K_D}{8}\left[1 + 8\frac{[a_T]}{K_D} - 1\right].$$

We wish to thank Olivier Landry and Miryam Elouneg-Jamroz for their collaboration in this project.

This work was supported by COFAA-IPN (México), EDI-IPN (México), CONACyT (México), MITACS (Canada), the Natural Sciences and Engineering Research Council (NSERC grant OGP-0036920, Canada), and Le Fonds pour la Formation de Chercheurs et l'Aide à la Recherche (FCAR grant 98ER1057, Québec).

REFERENCES

Ackers, G. K., A. D. Johnson, and M. A. Sea. 1982. Quantitative model for gene regulation by λ phage repressor. *Proc. Natl. Acad. Sci. USA*. 79:1129–1133.

Arkin, A., J. Ross, and H. H. McAdams. 1998. Stochastic kinetic analysis of developmental pathway bifurcation in phage λ-infected *Escherichia coli* cells. *Genetics*. 149:1633–1648.

Aurell, E., S. Brown, J. Johnson, and K. Sneppen. 2002. Stability puzzles in phage λ. *Phys. Rev*. E65:051914.

Aurell, E., and K. Sneppen. 2002. Epigenetics as a first exit problem. *Phys. Rev. Lett*. 88:048101.

Bremer, H., and P. P. Dennis. 1996. Modulation of chemical composition and other parameters of the cell by growth rate. *In Escherichia coli* and *Salmonella thyphymurium*: Cellular and Molecular Biology, Vol. 2. F. C. Neidhart, R. Curtis, J. L. Ingraham, E. C. C. Lin, K. B. Low, B. Magasanik, W. S. Reznikoff, M. Riley, M. Schaechter, and H. E. Umbarger, editors. American Society for Microbiology, Washington, DC. 1553–1569.

Burz, D., D. Becket, N. Benson, and G. K. Ackers. 1994. Self-assembly of bacteriophage λ CI repressor: effects of single-site mutations on the monomer-dimer equilibrium. *Biochemistry*. 33:8399–8405.

Court, D., B. Crombrugghe, S. Adhya, and M. Gottesman. 1980. Bacteriophage lambda Hin function II. Enhanced stability of lambda messenger RNA. *J. Mol. Biol*. 138:731–743.

Darling, P. J., J. M. Holt, and G. K. Ackers. 2000a. Couple energetics of λ *cro* repressor self-assembly and site-specific DNA operator binding. I: Analysis of *cro* dimerization from nanomolar to micromolar concentrations. *Biochemistry.* 39:11500–11507.

Darling, P. J., J. M. Holt, and G. K. Ackers. 2000b. Coupled energetics of λ *cro* repressor self-assembly and site-specific DNA operator binding. II: Cooperative interactions of *cro* dimers. *J. Mol. Biol.* 302:625–638.

Dodd, I. B., A. J. Perkins, D. Tsemitsidis, and B. Egan. 2001. Octamerization of λ CI repressor is needed for repression of P_{RM} and efficient switching from lysogeny. *Genes &. Development.* 15:3013–3022.

Draper, D. E. 1996. Translational initiation. *In Escherichia coli* and *Salmonella thyphymurium*: Cellular and Molecular Biology, Vol. 1. F. C. Neidhart, R. Curtis, J. L. Ingraham, E. C. C. Lin, K. B. Low, B. Magasanik, W. S. Reznikoff, M. Riley, M. Schaechter, and H. E. Umbarger, editors. American Society for Microbiology, Washington, DC. 902–908.

Fong, R. S., S. Woody, and G. N. Gussing. 1994. Direct and indirect effects of mutations in λ P_{RM} on open complex formation at the divergent P_R promoter. *J. Mol. Biol.* 240:119–120.

Giladi, H., M. Gottesman, and A. B. Oppenheim. 1990. Integration host factor stimulates the phage lambda pL promoter. *J. Mol. Biol.* 213: 109–121.

Gottesman, M. 1999. Bacteriphage λ: The untold story. *J. Mol. Biol.* 293:177–180.

Hawley, D. K., A. D. Johnson, and W. R. McClure. 1985. Functional and physical characterization of transcription initiation complexes in the bacteriophage λ O_R region. *J. Biol. Chem.* 260:8618–8626.

Hwang, J. J., S. Brown, and G. N. Gussin. 1988. Characterization of a doubly mutant derivative of the lambda P_{RM} promoter. Effects of mutations on activation of P_{RM}. *J. Mol. Biol.* 200:695–708.

Kennell, D., and H. Riezman. 1977. Transcription and translation initiation frequencies of the *Escherichia coli lac* operon. *J. Mol. Biol.* 114:1–21.

Leiv, L., and V. Kollin. 1967. Utilization and degradation of lactose operon mRNA in *Escherichia coli*. *J. Mol. Biol.* 24:247–259.

Li, M., W. R. McClure, and M. Susskind. 1997. Changing the mechanism of transcriptional activation by phage λ repressor. *Proc. Natl. Acad. Sci. USA.* 94:3691–3696.

Little, J. W., D. P. Shepley, and D. W. Wert. 1999. Robustness of a gene regulatory circuit. *EMBO J.* 18:4299–4307.

McAdams, H. H., and L. Shapiro. 1995. Circuit simulation of genetic networks. *Science.* 269:650–656.

Meyer, B. J., R. Maurer, and M. Ptashne. 1980. Gene regulation at the right operator (O_R) of bacteriophage lambda. II. O_R1, O_R2, and O_R3: Their roles in mediating the effects of repressor and *cro*. *J. Mol. Biol.* 139: 163–194.

Pakula, A. A., V. B. Young, and R. T. Sauer. 1986. Bacteriophage lambda *cro* mutations: effects on activity and intracellular degradation. *Proc. Natl. Acad. Sci. USA.* 83:8829–8833.

Ptashne, M. 1986. A Genetic Switch, Gene Control and Phage Lambda. Cell Press, Cambridge, MA.

Ptashne, M., and A. Gann. 2000. Genes & Signals. Cold Spring Harbor Laboratory Press, New York.

Reinitz, J., and J. R. Vaisnys. 1990. Theoretical and experimental analysis of the phage lambda genetic switch implies missing levels of cooperativity. *J. Theor. Biol.* 145:295–318.

Rozanov, D. V., R. D'Ari, and S. P. Sineoky. 1998. RecA-independent pathways of lambdoid prophage induction in *Escherichia coli*. *J. Bacteriol.* 180:6306–6315.

Shea, M. A., and G. K. Ackers. 1985. The O_R control system of bacteriophage lambda, a physical-chemical model for gene regulation. *J. Mol. Biol.* 181:211–230.